ATOMIC VELOCITY DISTRIBUTIONS OUT OF HYDROGEN MASER DISSOCIATORS

Bernardo Jaduszliwer and Yat C. Chan
Chemistry and Physics Laboratory
The Aerospace Corporation
P.O. Box 92957, Los Angeles, CA 90009

Abstract

We have determined velocity distributions of atoms effusing out of RF discharge hydrogen dissociators, of the type used in hydrogen masers. This work was motivated by long–term reliability issues related to the possible use of masers as frequency standards on board satellites. Chief amongst these issues is the maser's hydrogen budget, since many of the common failure modes of a maser involve either the hydrogen source or sink. Since the focussing properties of the state–selecting magnets are velocity–dependent, the overall hydrogen budget will depend not only on the dissociation efficiency, but also the velocity distribution of the hydrogen atoms leaving the dissociator. Many times, that distribution has been tacitly assumed to be Maxwellian at wall temperature, but that assumption is not necessarily valid. Our measurements show the distributions to be much narrower than Maxwellian, and to broaden as the hydrogen pressure in the dissociator increases. Operating the dissociator to yield a relatively narrow velocity distribution and using a state–selecting magnet well matched to that distribution may significantly improve the efficiency of hydrogen use by the maser.

INTRODUCTION

The use of hydrogen masers as frequency standards on board spacecraft requires careful consideration of long–term reliability issues. Chief amongst them is the maser's hydrogen budget, since many of the common failure modes of a hydrogen maser involve either the hydrogen source (storage or dissociator) or sink (ion pump or getters). An excess of hydrogen atoms in the $F = 1$, $M = 0$ state must be continuously fed into the maser bulb. The ratio of the rates at which atoms in the proper hyperfine state enter the bulb and molecules are fed into the dissociator will impact strongly the maser's long–term reliability. This ratio will be determined mainly by the dissociator's efficiency and the properties of the state–selecting magnet. Atomic state–selection is performed in hydrogen masers by a quadrupole or hexapole magnet which focuses atoms in the $F = 1$, $M = 0$ state at the bulb's entrance orifice, and defocuses the $F = 0$, $M = 0$ ones. The focal length of those magnets depends strongly on atomic speed, and typically only a narrow range of atomic velocities will be focussed. Clearly, dissociators yielding narrower velocity distributions could make more efficient use of the hydrogen supply.

Relatively little is known of the velocity distribution of atoms effusing out of RF discharge hydrogen dissociators. In many cases the tacit assumption is made that the atoms will be in thermal equilibrium with the dissociator wall, but that is not necessarily the case. The threshold for molecular dissociation by collisions with discharge electrons is about 8.5 eV; since the molecular binding energy

is approximately 4.7 eV, each atom carries away an excess energy of about 2 eV[1]. Depending on dissociator geometry and gas density, the hydrogen atoms may, or may not, undergo enough gas and wall collisions to thermalize fully. Walraven and Silvera[2] have studied the characteristics of a beam of hydrogen atoms produced in a microwave discharge followed by a thermal accommodator and found the velocity distributions to be Maxwellian at the accommodator temperature. Hershcovitch et al.[3] studied a similar dissociator–and–accommodator combination, operated at higher pressures and flow rates, and measured velocity distributions in reasonable agreement with the calculated supersonic–flow ones. Since thermal accommodators are not commonly used in maser dissociators, these results are not directly applicable to our problem. Miller[4] investigated a helium–cooled microwave discharge dissociator at relatively high pressure (3.3 Torr) and measured a velocity distribution which was slightly narrower than the Maxwellian at the estimated discharge temperature. We are studying the velocity distributions of atomic hydrogen produced in an RF discharge dissociator having a geometry and operating parameters resembling those of a maser dissociator. This paper discusses the experimental technique and presents our preliminary results.

EXPERIMENTAL APPARATUS

Atomic hydrogen velocity distributions have been determined using a magnetic deflection technique. Figure 1 shows the experimental arrangement. Hydrogen is fed through a standard, temperature–controlled Pd–Ag alloy leak[5] into a cylindrical double–walled Pyrex bulb, 15 cm long, 1.9 cm internal diameter and 3.8 cm outside diameter. Compressed air flows between the walls to provide cooling, and RF power is inductively coupled to the discharge through an external 25–turn coil. The hydrogen beam exits the dissociator through a 0.1 cm long, 0.025 cm wide slit, is collimated by a second slit, 0.025 cm wide, set at d= 63.7 cm away from the source slit, and then travels between the polepieces of an L= 11.4 cm long electromagnet configured in the "two–wire" geometry described by Rabi et al.[6]. After additional travel through a D= 71.3 cm drift tube, the beam is detected by a quadrupole mass analyzer.

Molecular hydrogen, having no magnetic dipole moment, will travel through the magnet without deflection, but the hydrogen atoms will be deflected by the inhomogeneous magnetic field. The dissociator is attached to the rest of the apparatus by flexible vacuum bellows, and can be displaced transversally by micrometer screws; in this way, the angular distribution of atoms deflected by the field can be measured.

ATOMIC DEFLECTION IN A "TWO–WIRE" MAGNETIC FIELD

An atom having magnetic moment $\vec{\mu}$, immersed in a magnetic field $\vec{H}$, has an energy $E = -\vec{\mu} \cdot \vec{H}$. The force acting on the atom is $\vec{F} = \mathrm{grad}(\vec{\mu} \cdot \vec{H}) \approx \mu_{eff}\mathrm{grad}(H)$, where μ_{eff} is the component of the atomic magnetic moment along the field direction. In general, μ_{eff} will depend on the atomic ground state quantum numbers and the magnetic field strength. If an atom has total electron angular momentum $J = 1/2$ and nuclear spin I, both in units of $h/2\pi$ then its effective magnetic moment is given by Breit–Rabi's formula[7],

$$\mu_{eff} = \pm \frac{\epsilon + 2M/(2I+1)}{[1 + 4M\epsilon/(2I+1) + \epsilon^2]^{1/2}} \mu_0, \qquad (1)$$

where the $(+)$ sign corresponds to total angular momentum $F = I - 1/2$, the $(-)$ sign to $F = I + 1/2$ and M is the total azimuthal quantum number. ϵ is proportional to the ratio of magnetic–to–hyperfine

energy, $\epsilon = g\mu_0 H/W$, where g is the Lande factor for the atom, μ_0 is the Bohr magneton and W the atomic hyperfine splitting.

Figure 2 shows the cross section of the "two-wire" magnet; 2α is the separation between the "equivalent wires"[8]. If a narrow atomic beam enters the magnet at $X = 1 \cdot 2\alpha$ (as determined by the collimating slit) and the atomic transversal displacements within the magnet are small, then the force acting on the atoms remains approximately constant[9], and so does the acceleration:

$$a \approx \frac{0.984}{\alpha} \frac{\mu_{eff}}{m} H\hat{i}, \tag{2}$$

where H is the magnetic field intensity at the atomic beam, m is the atomic mass and $\hat{i}$ a unit vector pointing along the x-axis. Under these conditions, the trajectory equations for the atoms traveling from source to detector can be solved easily. With no magnetic field, an atom of magnetic moment μ_{eff} and speed V leaving the source slit at X_S will be detected at $X_D = -X_S(L+D)/d$. If now the field is set at H and the detector is not moved, an identical atom will have to leave the plane of the source slit at X'_S, given by

$$X'_S \approx X_S + \frac{a}{V^2} \frac{Ld}{2} (1 + \frac{D}{L+D}) \tag{3}$$

in order to be detected. If $f_0(X_S)$ is the distribution of detected atoms as a function of source slit position at zero magnetic field, and $g(V)$ the speed distribution of atoms leaving the source slit, then the distribution of detected atoms at non-zero field, $f(X_S)$, will be given by

$$f(X_S) \approx \sum_{F,M} \int_0^\infty f_0(X_S - K_{FM}/V^2) g(V) dV, \tag{4}$$

where

$$K_{FM} = \frac{0.492}{\alpha} \frac{\mu_{eff}}{m} HLd(1 + \frac{d}{L+D}). \tag{5}$$

Both $f_0(X_S)$ and $f(X_S)$ can be measured, and then Eq. (4) can be used to verify whether a given velocity distribution is consistent with these measured distributions.

CALIBRATION AND PROOF-OF-CONCEPT EXPERIMENT

A preliminary experiment to study the deflection of a rubidium beam was performed in order to calibrate the electromagnet and test the use of Eq. (4) to verify an assumed velocity distribution.

Equation (1) shows that for an atom having nuclear spin I, $\mu_{eff} = 0$ if $\epsilon = -2M/(2I+1)$. At field intensities determined by

$$H = \frac{-M}{2I+1} \frac{W}{\mu_0}, \tag{6}$$

atoms with $M < 0$ will not be deflected by the field. Natural rubidium is a mixture of 72.2% Rb_{85} ($I = 5/2$) and 27.8% Rb_{87} ($I = 3/2$). Rb_{85} will have zero effective moments at $H = 361\ G$ ($M = -1$) and $H = 722\ G$ ($M = -2$). Rb_{87} will have a zero effective moment at $H = 1221\ G$ ($M = -1$). Figure 3 shows the detected atomic signal as a function of magnet coil current, with the rubidium beam source and detector on the apparatus axis. At the field values listed above, atoms in the zero effective moment states will travel through the magnet without deflection, leading to an increased signal. The effect of the zero effective moment states can be made more apparent on the figure by subtracting from each one of the marked features the local sloping background. The peaks labeled A and B can then

be identified with the zero effective moments at 722 G and 1221 G, respectively, yielding a calibration of 66.3 G/A for the magnet.

The rubidium source for these measurements was a two–chambered oven designed an operated to insure effusive flow; under those conditions, the atomic beam speed distribution should be beam–Maxwellian,

$$g(V) = (2/\beta)(V/\beta)^3 \exp[-(V/\beta)^2], \tag{7}$$

where $\beta = \sqrt{(2kT/m)}$, and T is the oven temperature. We measured $f(X_S)$ for $H = 1061\ G$, 1220 G and 1525 G, as well as $f_0(X_S)$, and then used Eq. (4), with the speed distribution given by Eq. (7), to calculate the expected $f(X_S)$ at those field values. The results are presented on Figure 4. For $x < 0$ the agreement between calculated and measured detected atom distributions is somewhat poor; this is the convex polepiece side of the magnet, and the constant–force approximation made to derive Eq. (3) breaks down for atoms traveling too close to the polepiece. For $x > 0$, the agreement between calculated and measured $f(X_S)$ is excellent; these results fully validate our experimental technique.

ATOMIC HYDROGEN VELOCITY DISTRIBUTIONS

Figure 5 shows the atomic hydrogen beam fraction as a function of total pressure in the dissociator bulb, and discharge RF power. These data were obtained at 205 MHz; the discharge power was corrected for reflection, and the atomic fraction, measured with the quadrupole mass analyzer, was corrected for the H^+ background when detecting H_2.

We have taken preliminary atomic hydrogen deflection data at total dissociator pressures of 0.2, 0.4 and 0.7 Torr, and at 995 and 1326 G magnetic fields. Zero field detected atom distributions have also been measured at each operating pressure. We then used Eq. (4) with the beam–Maxwellian distribution given by Eq. (7) to test the validity of the hypothesis of a thermal beam; the source temperature T was treated as a free parameter. Figure 6 shows, as an example, the deflection data at 995 G and 0.4 Torr, together with the expected detected atom distributions for Maxwellian beams at 300 K and 500 K. Bearing in mind that, as shown by Eq. (3), the transversal atomic displacement by the field is inversely proportional to V^2, it is clear that the distribution at 300 K contains a large excess of slow atoms (large deflections), while the distribution at 500 K contains a correspondingly large excess of fast atoms (small deflections). Similar problems were encountered when analyzing the rest of the deflection data. These results show that the atomic velocity distribution in the beam must be significantly narrower than the beam–Maxwellian.

In order to estimate qualitatively the characteristics of the actual velocity distribution in our atomic hydrogen beam, we decided to model it by a Gaussian distribution of peak speed V_0 and standard deviation σ,

$$g(V) = \frac{1}{\sigma\sqrt{2\pi}} \exp\left[-(V - V_0)^2/2\sigma^2\right]. \tag{8}$$

V_0 and σ were treated as free parameters and adjusted to provide a reasonable approximation to the measured deflection data. Given the preliminary nature of the deflection data and model velocity distribution, no attempt was made to obtain a "best fit". Figures 7, 8 and 9 show the deflection data at 995 G for dissociator total pressures of 0.2, 0.4 and 0.7 Torr, with the corresponding results calculated using the velocity distributions given by Eq. (8). A much closer agreement with the measured data is obtained than when using Maxwellians. Similar results were obtained for the data at 1326 G.

DISCUSSION AND CONCLUSIONS

The Gaussian velocity distributions used to calculate the results presented in Figures 7–9 are presented in Figures 10, 11 and 12, together with the corresponding Maxwellians having the same peak velocity. They show that the atomic beam velocity distributions are indeed non–thermal, and much narrower than Maxwellians. Since the distribution at 0.7 Torr is broader than the distributions at 0.2 and 0.4 Torr, it is also clear that we are not measuring distributions narrowed by gas–dynamics effects. Instead, incomplete thermalization of the hydrogen atoms must be the cause; this interpretation is consistent with the width of the distribution becoming closer to the Maxwellian width as the discharge pressure increases.

The peak velocities correspond to kinetic energies of about 0.06 eV, much smaller than the approximately 2 eV of kinetic energy available per atom immediately after dissociation. Since the atoms must lose the excess energy without broadening significantly their energy distribution, the main energy–loss mechanism must be an inelastic process with a relatively large energy loss per collision; vibrational excitation of the background hydrogen molecules, (0.546 eV/collision) seems to be a good candidate. Further studies in this area are required.

It is well known that the velocity passband of the hexapole or quadrupole magnets used as state selectors in hydrogen masers is rather narrow (about 25% FWHM). Our findings indicate that it should be possible to design the state–selecting magnet having a velocity passband which matches as closely as possible the fairly narrow velocity distribution of the hydrogen atoms effusing out of the dissociator, thus greatly enhancing the efficiency with which the maser uses its hydrogen supply.

REFERENCES

1. S. J. B. Corrigan and A. von Engel, "Excitation and Dissociation of Hydrogen by an Electron Swarm", Proc. Roy. Soc. A, 245, 335 (1958).

2. J.T. M. Walraven and I. F. Silvera, "Helium–Temperature Beam Source of Atomic Hydrogen", Rev. Sci. Instrum. 53, 1167 (1982).

3. A. Hershcovitch, A. Kponou and T. O. Niinikoski, "Cold High–Intensity Atomic Hydrogen Beam Source", Rev. Sci. Instrum. 58, 547 (1987).

4. T. M. Miller, "Atomic Beam Velocity Distributions with a Cooled Discharge Source", J. Appl. Phys. 45, 1713 (1973).

5. J. Viennet, P. Petit and C. Audoin, "Regulateur de Debit d'Hydrogene a Reponse Rapide", J. Phys. E 6, 261 (1973).

6. I. I. Rabi, J. M. B. Kellogg and J. R. Zacharias, "The Magnetic Moment of the Proton", Phys. Rev. 46, 157 (1934).

7. G. Breit and I. I. Rabi, "Measurement of Nuclear Spin", Phys. Rev. 38, 2082 (1931).

8. N. F. Ramsey, "Molecular Beams" (Oxford University Press, New York, 1956), p. 400.

9. N. F. Ramsey, ibid., p. 398.

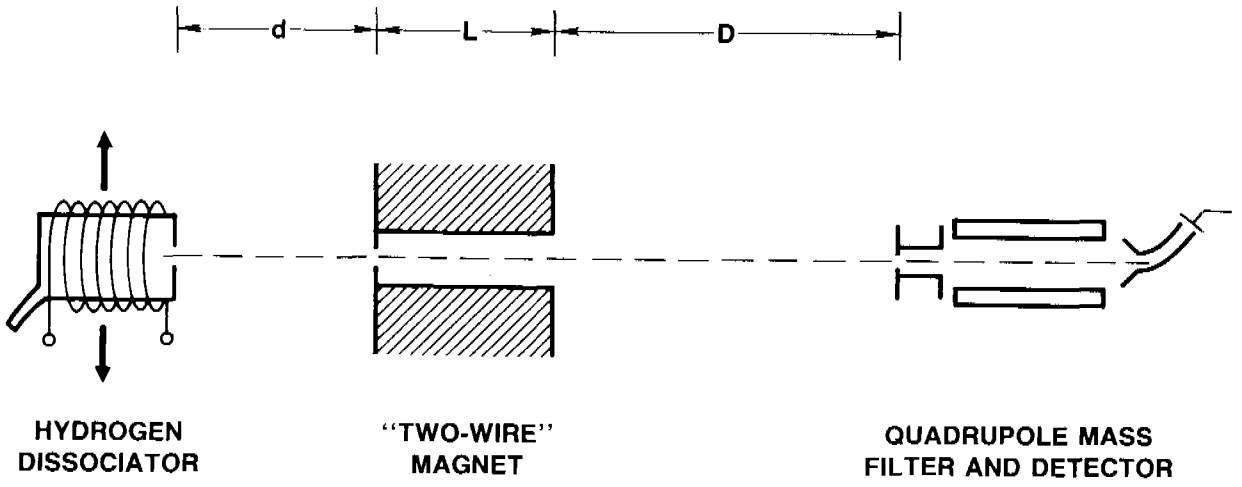

Fig.1: Schematic view of the experimental arrangement. The hydrogen dissociator can be displaced transversally.

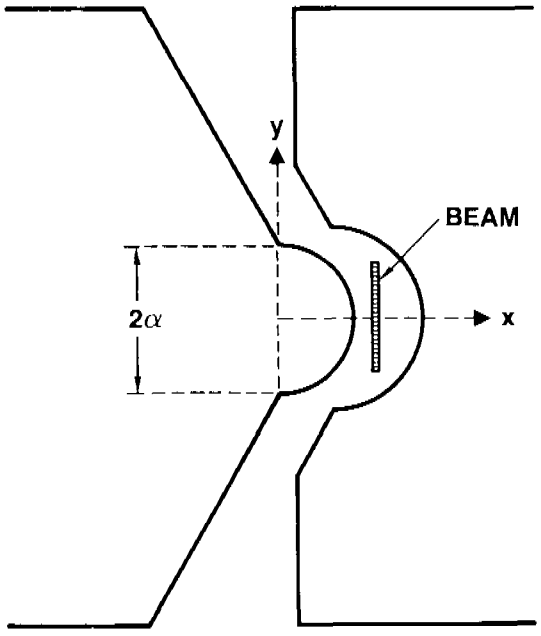

Fig.2: Cross section of the "two-wire" field magnet. 2α is the separation of the "equivalent wires".

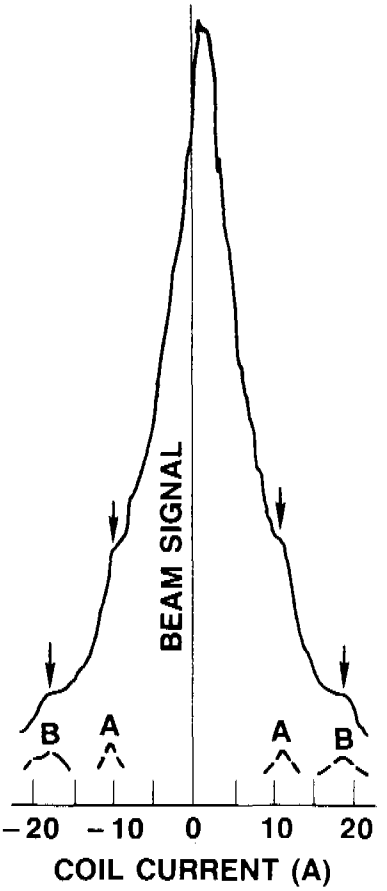

Fig. 3: Rubidium atomic beam signal (detector and oven on axis) vs. magnet coil current. Arrows show features due to zero effective moment states. Dashed lines were obtained by substracting the local constant-slope background from each feature. A: Rb_{85}, M=-2; B: Rb_{87}, M=-1.

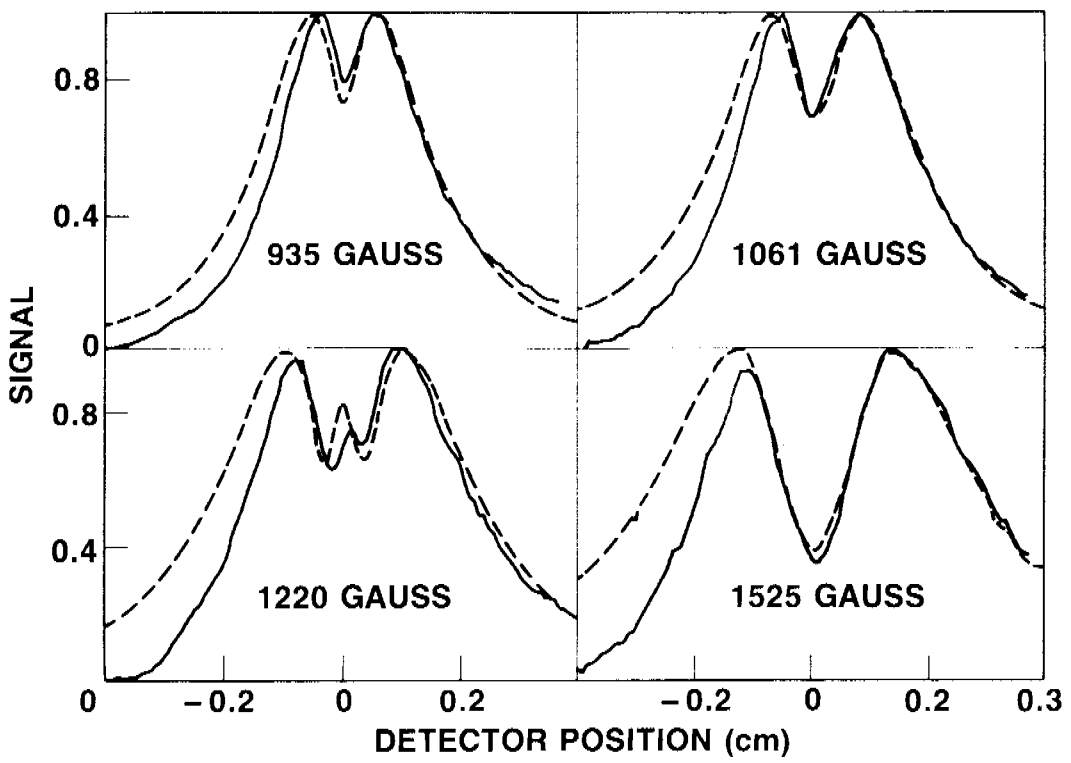

Fig.4: Detected rubidium atom distributions at indicated magnetic fields. Oven temperature: 484 K. Full line: measured. Dotted line: calculated for a Maxwellian beam.

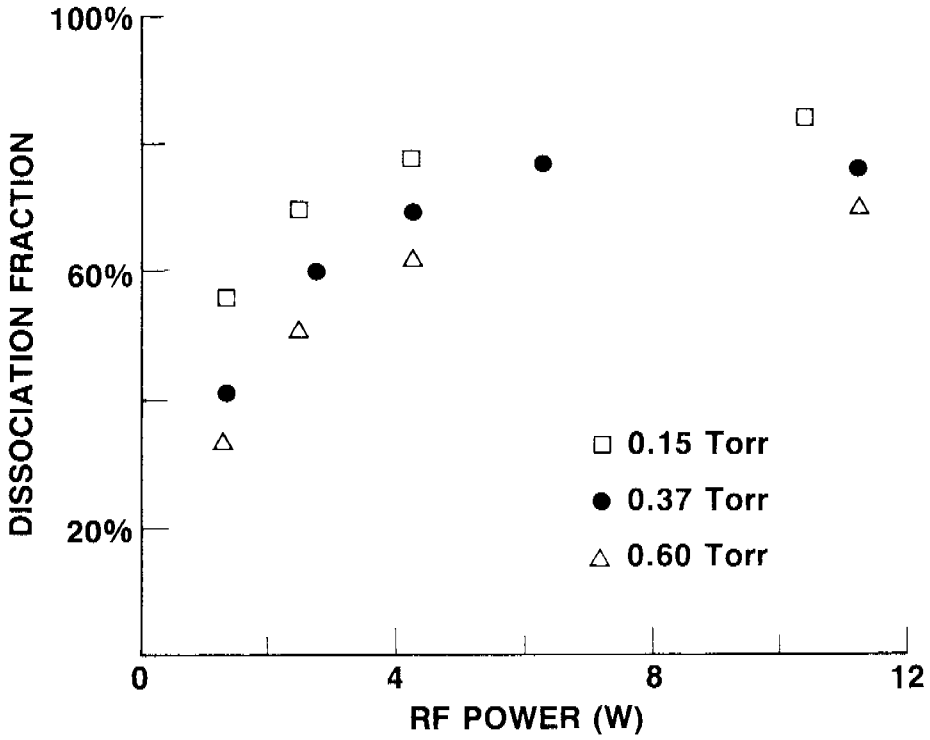

Fig.5: Atomic hydrogen beam fraction vs. rf discharge power. Total dissociator bulb pressures are indicated.

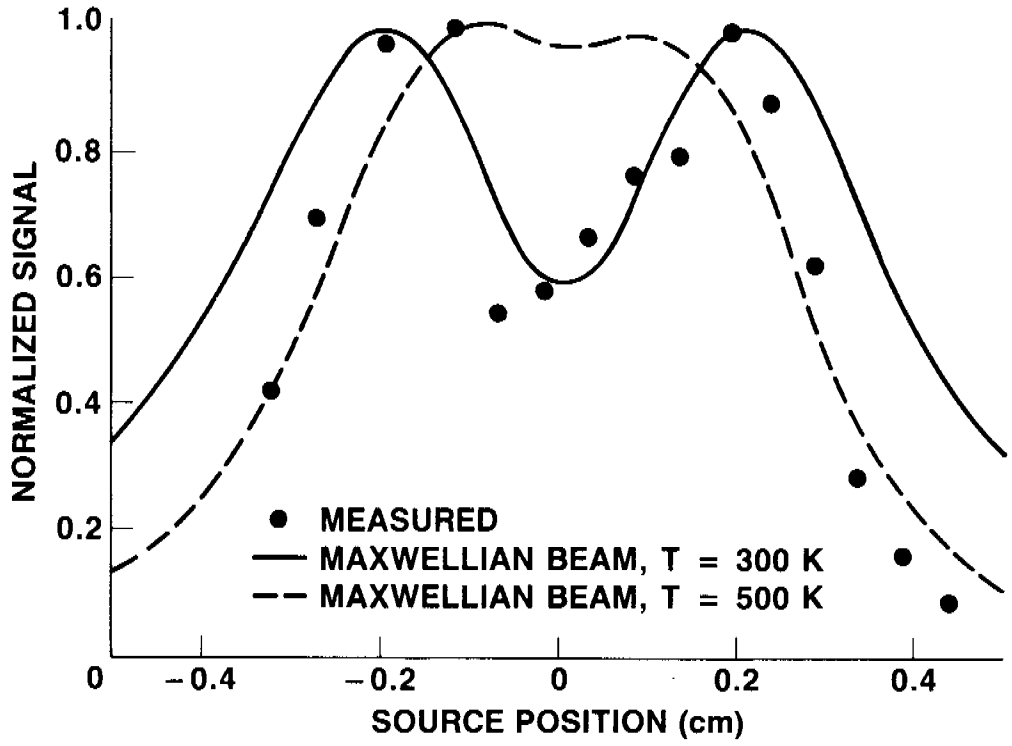

Fig.6: Detected hydrogen atom distribution, at 995 G and 0.40 Torr. Dots: measured. Curves: calculated.

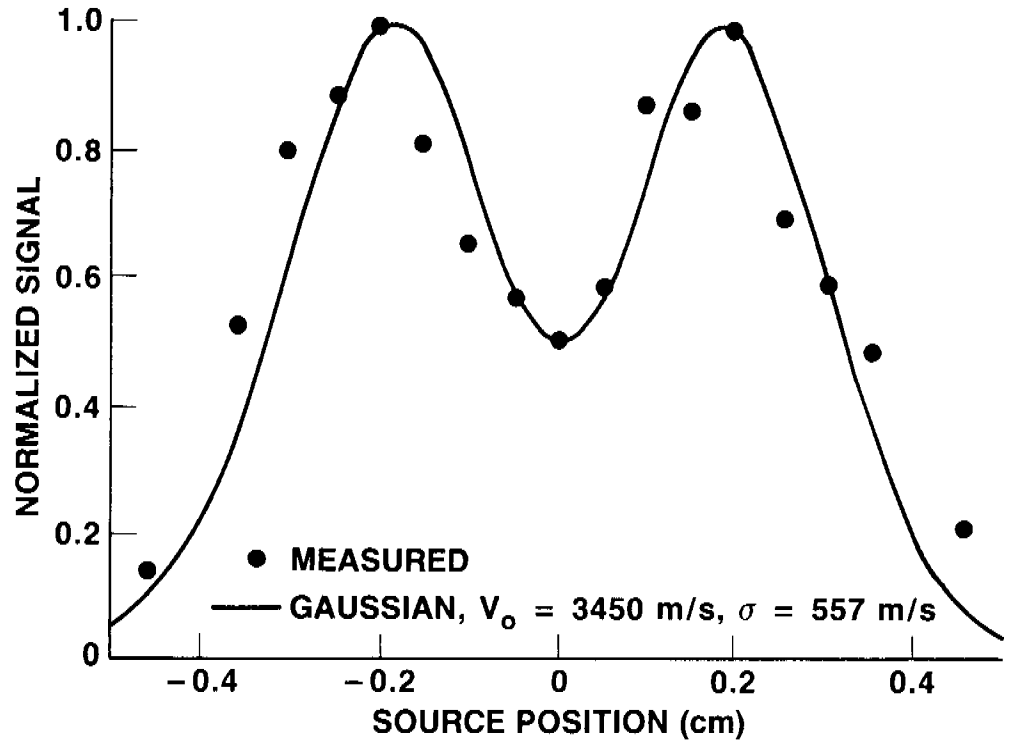

Fig.7: Detected hydrogen atom distribution, at 995 G and 0.20 Torr. Dots: measured. Curve: calculated.

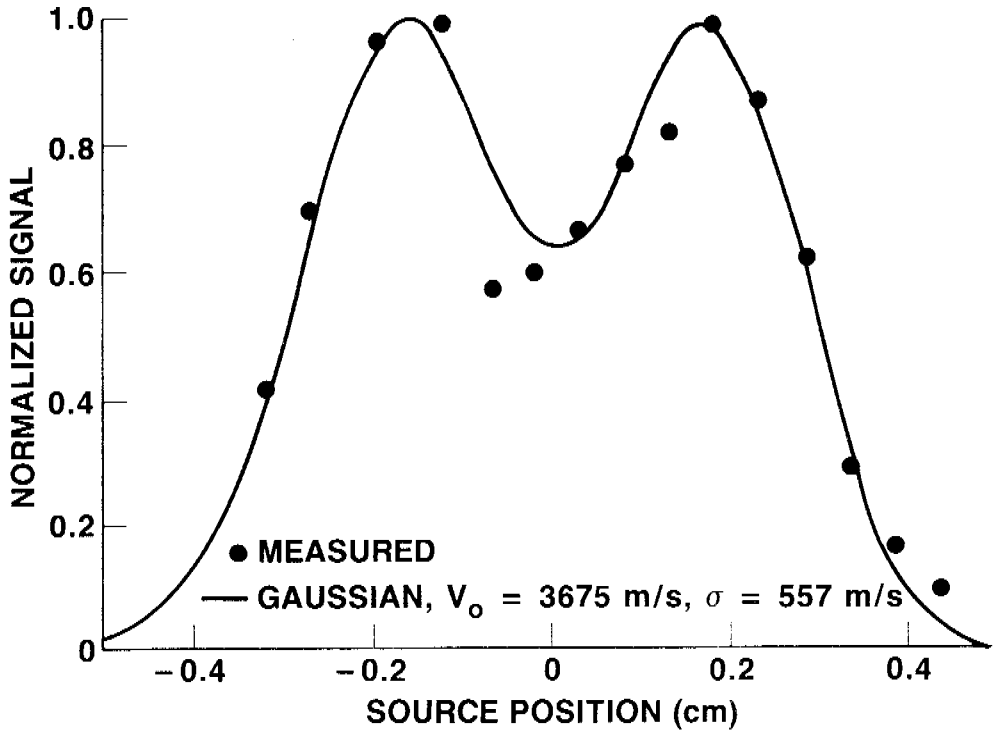

Fig.8: Detected hydrogen atom distribution, at 995 G and 0.40 Torr. Dots: measured. Curve: calculated.

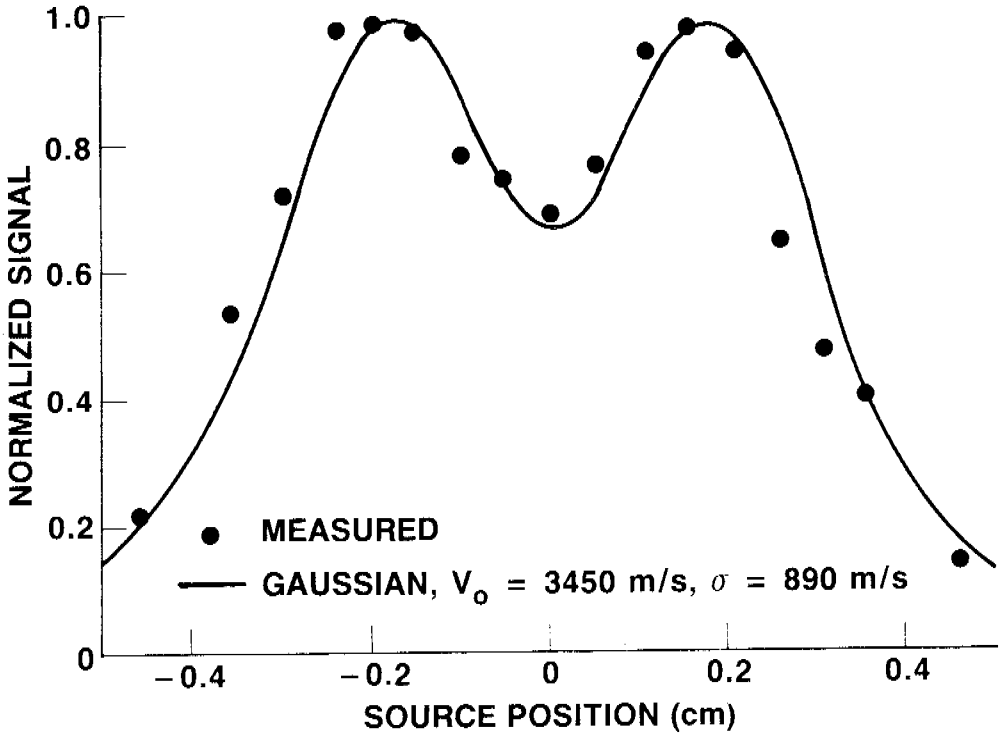

Fig.9: Detected hydrogen atom distribution, at 995 G and 0.70 Torr. Dots: measured. Curve: calculated.

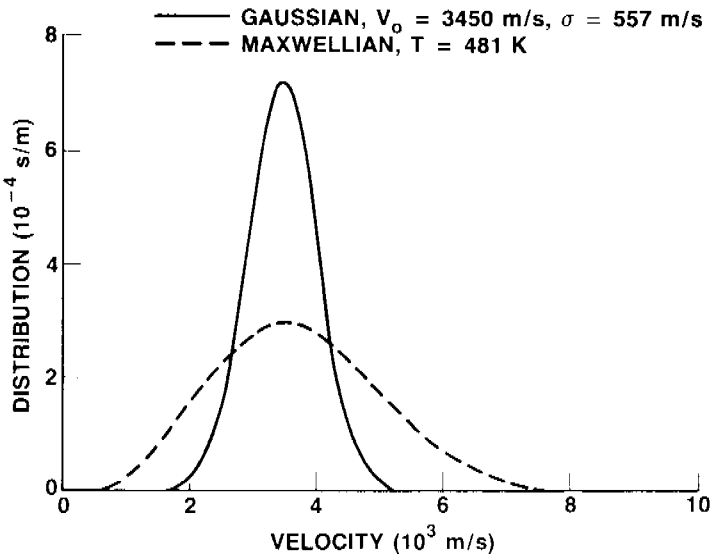

Fig. 10: Ful line: Gaussian velocity distribution used for Fig. 7. Dashed line: beam-Maxwellian distribution having the same peak velocity.

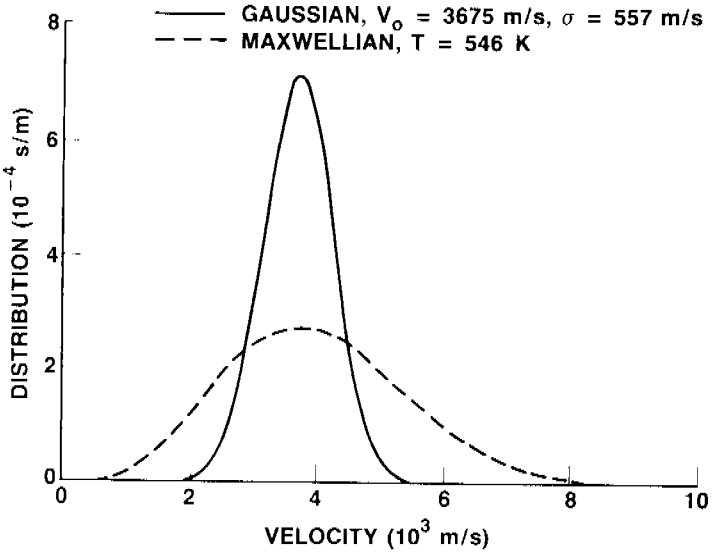

Fig. 11: Full line: Gaussian velocity distribution used for Fig. 8. Dashed line: beam-Maxwellian distribution having the same peak velocity.

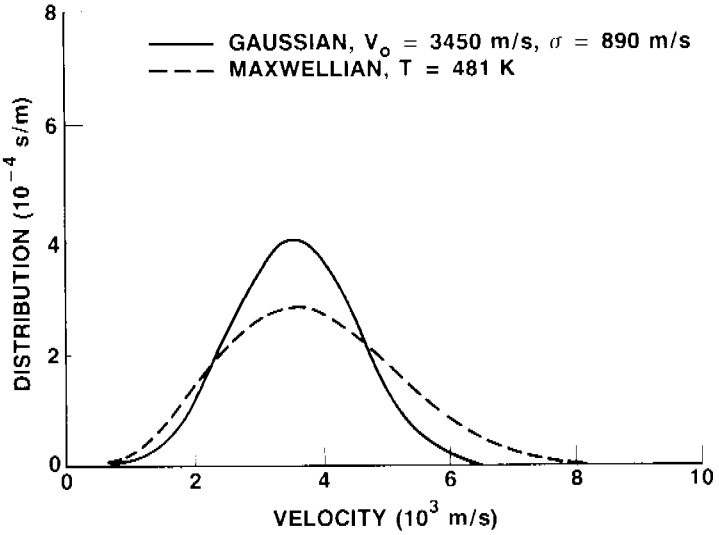

Fig. 12: Full line: Gaussian velocity distribution used for Fig. 9. Dashed line: beam-Maxwellian distribution having the same peak velocity.